THRUST FAULTING ON VENUS: TECTONIC MODELING OF THE VEDMA DORSA RIDGE BELT

S.A. Moruzzi[1,2] and W.S. Kiefer[2], [1]Cornell University, Department of Earth and Atmospheric Science, sam466@cornell.edu [2]Lunar and Planetary Institute, Universities Space Research Association, Houston, TX 77058

Introduction: Radar images from the Magellan mission reveal the presence of networks of ridge belts in several low-lying plains on Venus, including Atalanta Planitia, Vinmara Planitia, Lavinia Planitia, and Rusalka/Llorona/Vellamo Planitiae These ridge belts transect low lying plains and have been interpreted to the be the result of crustal convergence and thus faulting and folding over cold downwelling mantle [1-5]. They are distinct from wrinkle ridges, which are ubiquitous on the Venus plains but typically less than 2 km wide with limited topographic relief [6-7].

We center our study on Vedma Dorsa, an ~1700 km ridge belt where the ridges are approximately 30-70 km wide, 0.5-1 km high and commonly asymmetric in topographic cross-section. In this study, we perform elastic dislocation modeling of thrust faulting at several locations along Vedma Dorsa in order to constrain fault parameters such as fault displacement, faulted layer thickness, and fault dip. Our results support the interpretation that the ridge belts are formed by thrusting faulting and provide an improved understanding of the lithospheric properties and conditions under which these ridges formed.

Method: Magellan synthetic aperture radar (SAR) data provides detailed images of these ridge belts at approximately 120 m/pixel resolution (Figure 1A). In the SAR data, these features appear as radar bright structures that linearly trend NE-SW. Topographic scarps that face west are bright in the radar image while topographic slopes that face east are relatively dark. The sharp changes in radar brightness across the ridge belts are consistent with the interpretation of faulting as the dominant formation mechanism [3].

We mapped all of the ridge belts in Rusalka, Llorona and Vellamo Planitiae present in the Magellan SAR data. Based on this mapping, we selected Vedma Dorsa in Llorona and Vellamo Planitiae for detailed modeling because the available stereo topography data [8] (horizontal resolution of ~1-2 km) allows quantitative modeling at several locations. At each study site, we took five topography profiles perpendicular to the trend of the ridge belt, separated by 3-4 km along the ridge belt axis, and used their average as a representative topographic profile for that part of the ridge belt.

We modeled thrust faulting as elastic dislocations using Coulomb 3.3 [9-10]. We assumed Young's modulus of 80 GPa and Poisson's ratio of 0.25 for Venus's lithosphere, which are comparable to values for the terrestrial lithosphere. Our results are not sensitive to the specific value of coefficient of friction along the fault in the range 0.4-0.8, so we assumed the default value of 0.4 in the results shown here. In order to avoid unphysical discontinuities in the stress at the edges of the fault zone, we applied a linear taper to the imposed displacement, consistent with the suggested tapering for the program. We produced models for a faulted layer thickness, *T*, from 10 km to 45 km with a step size of 5 km, displacement along the fault, *D*, from 0 km to 3 km with a step size of 0.2 km, and fault dip angle θ from 25° to 35° with a step size of 5°. In some cases, we considered a listric fault, in which the fault dip decreases with depth (Figure 1B), or a blind fault.

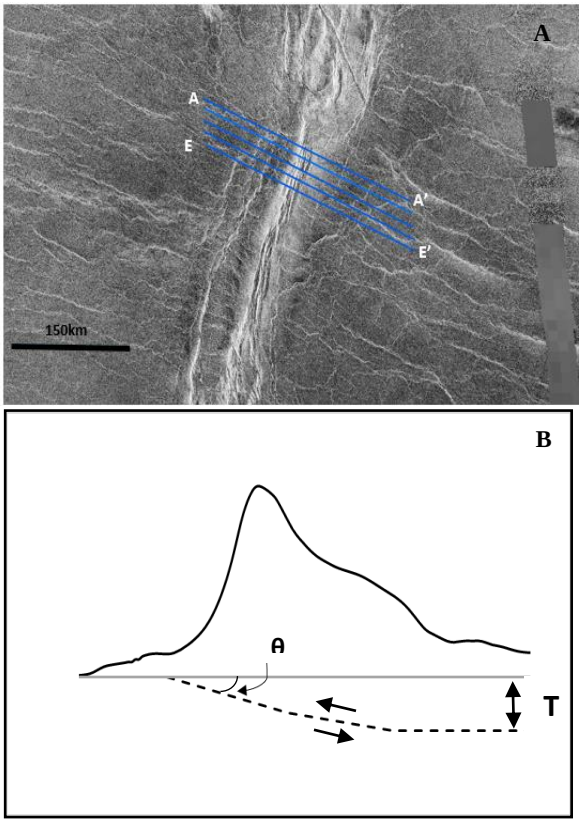

Figure 1: A) **Magellan SAR image (~120m/pixel) of Site 1 (28.4°N, 159.3°E). Five topography profiles were taken across ridge belt and are shown in blue.** ***B)*** **Observed topography of Site 1 corresponding to profiles in *A* with the best fit listric fault model. Θ is the dip of the fault plane and T is faulted layer thickness. Faulted layer thickness is not to scale**

Results: Three segments of the Vedma Dorsa belt were chosen for analysis. The ridge for which the most comprehensive modeling was done (Site 1; radar in Figure 1, topography in Figure 1 & 2) has a relief of approximately 0.8 km. The most prominent radar bright structure in Figure 1A corresponds to the steep

western scarp face on the observed topography profile in Figure 1B. Along much of the ridge, there are 3 additional closely spaced (~1 km separation), sharply defined lineations that occur near the crest of the ridge. We interpret these as secondary faults.

We fit the observed topography with predicted models in order to find the best fit parameters for the thrust fault for Site 1 (Figure 2). A 25° dip of the fault plane, consistent with the dip of a thrust fault, provides a good fit. We varied faulted layer thickness while holding displacement along the fault and dip angle of the fault plane constant (Figure 2A). Faulted layer thickness of ~10-20 km allows for the best fit to the observed topography. We also varied the displacement along the fault while holding the dip of the fault plane and faulted layer thickness constant (Figure 2B). A fault displacement of 1.4-1.5 km gives the best fit to the observed topography.

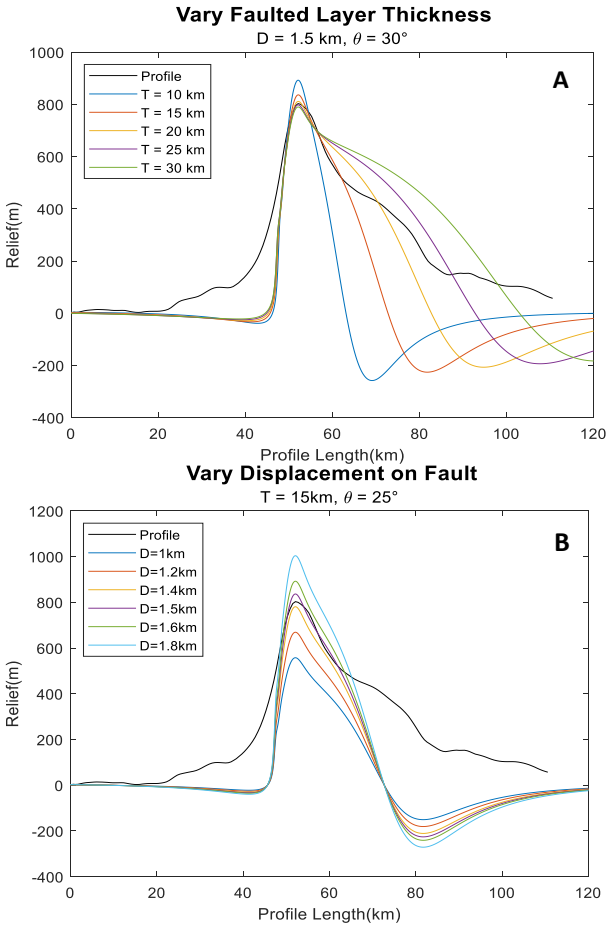

Figure 2: **Comparison of observed topography to predicted non-listric fault models for Site 1. A) Variation in faulted layer thickness while displacement on the fault (*D*) and dip of the fault plane(*θ*) are held constant. B) Variation in displacement on fault while faulted layer thickness(*T*) and *θ* are held constant.**

Adding complexities to the fault model improves the fit to the periphery of the observed topography. A blind fault model whose upper tip is 3-6 km below the surface results in increased deformation in the foreslope region at distances of 20-50 km along the profile and improves the fit to the topography in that area. Allowing the fault to be listric with 10-20 km faulted layer thickness and 1-2 km offset increases the surface uplift and improves the fit to the observed topography between 60 and 80 km along the profile. Models in which the displacement varies with depth on the listric fault have also been suggested for Mars [11].

We have studied two additional segments of Vedma Dorsa, both of whose topography show evidence of a back-thrust accompanying the main thrust fault [12]. Quantitative modeling has been completed for Site 2 (37.7° N, 152.6°E). The best fit for faulted layer thickness is between 10 and 15 km for both thrust faults. A displacement along the fault of 0.6 km and fault dip of 30° fits the first thrust fault while a displacement of 0.4 km and fault dip of 25° fits the second thrust fault. Preliminary modeling for Site 3 (41.4° N, 158.8°E) suggests a faulted layer thickness of ~15-20 km and offsets between ~1-1.5 km.

In summary, our results for the three modeling sites are consistent with thrust faulting as the dominant mechanism for producing Vedma, with best fit parameters of D ~ 1-2 km, T ~10-20 km, and θ ~ 25-30°. The base of the faulted layer may be controlled by the lithosphere's brittle-ductile transition (BDT). Using a standard lithospheric strength envelope formulation [e.g., 13], we have modeled the brittle lithosphere using Byerlee's law and the ductile lithosphere as dry diabase [14]. Our results for the BDT are consistent with a thermal gradient of 5-9 K/km and a mantle heat flux of 15-27 mW m^{-2} at the time of faulting. The low value for the heat flux is consistent with compressional deformation over cold, downwelling mantle.

References: [**1**] Squyres et al. (1992) *JGR, 97*, 13,578-13,599. [**2**] Solomon et al. (1992) *JGR, 97*, 13199-13255. [**3**] Stofan et al. (1993) *Chapter 8 of Guide to Magellan Image Interpretation, JPL Publication 93-24*, pp. 93-108. [**4**] Young and Hansen (2005) *JGR, 110*, E03001. [**5**] Lawrence and Phillips (2003) *GRL, 30, 19*, 2003GL017515 [**6**] Billotti and Suppe (1999) *Icarus, 139*, 137-157. [**7**] Kreslavsky and Basilevsky (1998) *JGR, 103*, 11,103-11,111. [**8**] Herrick et al. (2012) *EOS, 93*, 125-126 [**9**] Toda et al. (2005) *JGR, 110*, B05S16. [**10**] Lin and Stein (2004) *JGR, 109*, B02303. [**11**] Watters et al. (2004) *Icarus 171*, 284-294. [**12**] Okubo and Schultz (2004) *GSA Bulletin, 116*, 594-605. [**13**] Kiefer and Li, GRL 36, 2009GL039827, 2009. [**14**] Mackwell et al., JGR 103, 975-984, 1998.